Alexandria Engineering Journal (2023) 72, 545–557

HOSTED BY

Alexandria University

Alexandria Engineering Journal

www.elsevier.com/locate/aej
www.sciencedirect.com

ORIGINAL ARTICLE

# Heat transfer analysis of Maxwell hybrid nanofluid with fractional Cattaneo heat flux

Hanifa Hanif [a,b,*], Liaquat Ali Lund [c], Rahimah Mahat [d], Sharidan Shafie [b,*]

[a] Department of Mathematics, Sardar Bahadur Khan Women's University, Quetta, Pakistan
[b] Department of Mathematical Sciences, Faculty of Science, Universiti Teknologi Malaysia, 81310 Johor Bahru, Johor, Malaysia
[c] KCAET Khairpur Mir's, Sindh Agriculture University TandoJam, Sindh, Pakistan
[d] Universiti Kuala Lumpur Malaysian Institute of Industrial Technology, Persiaran Sinaran Ilmu, Bandar Seri Alam, 81750 Masai, Johor, Malaysia

Received 12 February 2023; revised 29 March 2023; accepted 10 April 2023
Available online 21 April 2023

KEYWORDS

Hybrid nanofluid;
Cattaneo heat flux;
Maxwell fluid model;
Fractional derivative

**Abstract** Hybrid nanofluids are widely used to improve the efficiency of a thermal system in many aspects of engineering and science. Therefore, the current work is design to investigate the heat transfer of Cu-$Fe_3O_4$ nanoparticles in water base Maxwell fluid flow over a cone, which is kept in a porous medium. Additionally, the fluid experiences magnetic field and thermal radiation effects. As a result, the impacts of volume fraction, porosity, magnetic field, and thermal radiation are properly taken into account. It is observed that increasing temperature time relaxation with constant temperature fractional derivative decreases the thermal gradient, whereas increasing temperature fractional derivative parameter with constant time relaxation increases the thermal gradient. Moreover, adding 1% Cu-$Fe_3O_4$ increases the heat transfer rate of the fluid up to 1.13% and 1.24% when $Rd = 0$ and $Rd = 0.2$, respectively. On the other hand, the heat transfer rate of Maxwell fluid decreases up to 0.5% in the presence of a magnetic field specifically considering $M = 2$ without thermal radiation.



## 1. Introduction

A study of heat transfer analysis is one of the most important studies in fluid dynamics for engineers due to its almost universal application to various branches of science and engineering. The term "heat transfer" refers to the transfer of energy between regions caused by the random motion of atoms and molecules. It is important to keep in mind that convection, conduction, and radiation are the basic mechanisms of heat transfer in a heat transfer analysis. Among the methods of heat transfer, convection is one of the most important and is classified into natural convection (free convection) and forced and mixed convection. Convection occurs when a temperature gradient induces a density difference in the fluid, resulting in the fluid's flow. As a result of their poor heat transfer properties, these conventional fluids are required to be reprocessed in

* Corresponding authors.
E-mail addresses: hanifahanif@outlook.com (H. Hanif), sharidan@utm.my (S. Shafie).
☆ Peer review under responsibility of Faculty of Engineering, Alexandria University.

https://doi.org/10.1016/j.aej.2023.04.022

**Nomenclature**

| | |
|---|---|
| $(u, v)$ | velocity components in $(x, y)$ direction |
| $(x, y)$ | cartesian coordinates |
| $\mathscr{C}_1 - \mathscr{C}_6$ | nanofluid constants |
| $B_0$ | magnetic field strength |
| $C_p$ | specific heat capacity |
| $g$ | gravitational accelration |
| $Gr$ | thermal Grashof number |
| $K$ | non-dimensional porosity parameter |
| $k$ | thermal conductivity |
| $k_0$ | permiability of porous medium |
| $k_b$ | absorption parameter |
| $L$ | reference length |
| $M$ | non-dimensional magnetic parameter |
| $Nu_x$ | Nusselt number |
| $q$ | heat flux |
| $r$ | radius of the cone |
| $Rd$ | non-dimensional thermal radiation |
| $T$ | temperature |
| $t$ | time |
| Pr | Prandtl number |

**Greek Symbols**

| | |
|---|---|
| $\alpha$ | fractional order |
| $\beta$ | fractional order |
| $\beta_T$ | volumetric thermal expansion |
| $\Delta t$ | time step |
| $\Delta x$ | grid size in $x$ direction |
| $\Delta y$ | grid size in $y$ direction |
| $\lambda_1$ | momentum relaxation time |
| $\lambda_2$ | thermal relaxation time |
| $\mu$ | dynamic viscosity |
| $v$ | kinematic viscosity |
| $\rho$ | density |
| $\sigma$ | electrical conductivity |
| $\sigma_b$ | Steafen Boltzman coefficient |
| $\varphi$ | nanoparticles volume fraction |

**Subscripts/Superscripts**

| | |
|---|---|
| $*$ | non-dimensional |
| $f$ | base fluid |
| $hnf$ | hybrid nanofluid |
| $i$ | grid point in $x$ direction |
| $j$ | grid point in $y$ direction |
| $k$ | time level |
| $nf$ | nanofluid |
| $s$ | nanoparticles |

order to enhance their heat transfer properties when applied to engineering and industrial applications. The use of nanoscale particles, also called nanofluid, in the base fluid, was first introduced by Choi and Eastman [1]. Recent studies have demonstrated that the addition of solid nanoparticles can enhance thermal conductivity and affect suspension viscosity by 10%. In a study, the value thermophysical properties of nanofluids usually depend on certain factors such as size, shape, particle material, base fluid and concentration. They are the next generation of working fluids set to replace conventional fluids. It is reported in [2] that nanofluid velocity can be quantified as the sum of the relative velocity and the base fluid velocity. In addition, the thermophoresis and Brownian diffusion mechanisms are an integral part of the model provided by Buongiorno [2]. Several researchers have considered both models when analyzing convective transport in nanofluids. For instance, [3] considered the heat transfer flow of viscoelastic Walters'-B nanofluid through a circular cylinder by using Keller -box technique in convective and constant heat flux. Mat Noor et al. [4] examined magnetohydrodynamics (MHD) squeezing flow of Jeffrey nanofluid with a chemical reaction in a horizontal channel. Later, Asjad et al. [5] discussed and extended Mat Noor et al. [4] work by considering the same effect on the exponential stretching sheets. Hanif [6] investigated and analyze the heat and mass transfer in kerosene-based $\gamma$-oxide nanofluid using the finite difference method for cooling applications. Heat transfer over a stretching sheet on the MHD stagnation point flow of a nanofluid with radiation effects is analyzed by Ghasemi and Hatami [7]. References to nanofluids can widely be found in [8–11]. The latest development in nanofluid technology is hybrid nanofluids, in which suspended particles represent a complex combination of multiple nanoparticles. Hybrid nanofluids' purpose is to rectify mono nanofluids' shortcomings by using a contrasting property additive to overcome their disadvantages. To improve heat transfer distinctive, hybrid nanofluids are being utilized to balance the advantages and disadvantages of individual suspensions, attributed to their good aspect ratio, improved thermal network, and synergistic effects. In conclusion, the composite nanoparticles in hybrid nanofluids significantly increase thermal conductivity. A major challenge for practical applications may be long-term stability, production process, selection of appropriate nanomaterials combinations to create synergistic effects, and the cost of nanofluids. Therefore, it is a popular research topic to analyze heat transfer characteristics in hybrid nanofluids. Thirumalaisamy et al. [12] Compare the heat transfer of $Fe_3O_4$-MWCNT-water and $Fe_3O_4$-MWCNT-kerosene hybrid nanofluids using the non-Fourier heat flux mode. Hanif et al. [13] studied widely the applications of magneto–hybrid nanofluid flow past an absorptive cone in material engineering. Later, Hanif et al. [14] extended their work [13] and analyzed the hybrid model of Cu–$Fe_3O_4$/water nanofluid with PHF/PWT. However, Mohamed et al. [15] considered heat transfer of different base fluids, which is Ag-$Al_2O_3$/water hybrid nanofluid past a stretching sheet with Newtonian heating at a stagnation point. Ramzan et al. [16] presented a hybrid nanofluid model on an oscillating disk and studied the factor of nanoparticle shape and surface reaction. Gamachu and Ibrahim [17] extended the work of Ramzan et al. [16] by exploring the viscoelastic hybrid nanofluid model through a rotating disk. Shah et al. [18] presents the significance of suction and dual stretching on the dynamics of two different types of hybrid nanoflu-

ids. More discussion on hybrid nanofluid can be found in [19–21] Meanwhile, non-Newtonian fluids studies have generated considerable interest in recent years. Consequently, they are extensively used in industrial products. This has led to several non-Newtonian liquid models being proposed as a result. In addition to these models, the Maxwell fluid model has drawn the most attention. There are several constitutive equations that cannot be applied to such fluids. Due to the diversity of these fluids, various constitutive equations are proposed. Different types of non-Newtonian fluids can be divided into three categories: integral, rate, and differential. Non-viscous fluids are among the rate types of Maxwell fluid. Hanif et al. [22,23] investigated numerically the heat transfer of fractional Maxwell fluid past a vertical plate. Vieru et al. [24] investigated free convection flow of viscous fluids in a circular cylinder due to a generalized fractional thermal transport. Saqib et al. [25] extended the work and discussed heat transfer in the MHD flow of Maxwell fluid via the fractional Cattaneo–Friedrich model. As part of their research, Al Nuwairan et al. [26] investigated the numerical solution of Maxwell fluid with heat transfer through a porous medium as well as Soret-Dufour effects and thermophoretic particle deposition. It has been demonstrated by Fetecau et al. that the flow of Maxwell fluid through a porous plate channel can be numerically analyzed [27], while Loganathan et al. [28] have examined MHD flow of thermally radiative Maxwell fluid past a stretched sheet with Cattaneo–Christov dual diffusion. Zhang et al. [29] presented a study on memory effects on a conjugate buoyant convective transport of nanofluids. It should also be noted that Sadiq et al. [30] have developed some extensions of previous solutions to fractional Maxwell fluids. Some fruitful discussions on Maxwell fluid can be found in [31–35]. According to prior study, the flow of fractional Maxwell hybrid nanofluid past a permeable cone has not yet been studied. This study article considers the flow of fractional Maxwell hybrid nanofluid under the influence of magnetic field and thermal radiation to close this research gap. The fractional constitutive equations of Friedrich and Cattaneo for shear stress and heat conduction, respectively, are used in the mathematical modelling of the flow phenomena. The problem is approached for numerical solutions using the L1 algorithm and Crank-Nicolson numerical methods. The findings are displayed in graphs, and it is discussed how the relevant flow parameters affect fluid velocity and temperature distribution.

## 2. Mathematical formulation

Consider a two-dimensional unsteady flow of an incompressible Maxwell hybrid nanofluid over a vertical permeable cone. The $x$-axis is considered along the cone and the $y$-axis is assumed to be normal to the cone, see Fig. 1. A magnetic field of strength $B_0$ is applied in the $y$ direction. Using boundary layer assumptions and Boussinesq approximations, the continuity and momentum equations are given as [19]:

$$\frac{\partial}{\partial x}(ru)+\frac{\partial}{\partial y}(rv)=0, \tag{1}$$

$$\rho_{hnf}\left(\frac{\partial u}{\partial t}+u\frac{\partial u}{\partial x}+v\frac{\partial u}{\partial y}\right)=\frac{\partial \tau_{xy}}{\partial y}-\frac{\mu_{hnf}}{k_0}u-\sigma_{hnf}B_0^2u + g(\rho\beta_T)_{hnf}(T-T_\infty)\cos\gamma. \tag{2}$$

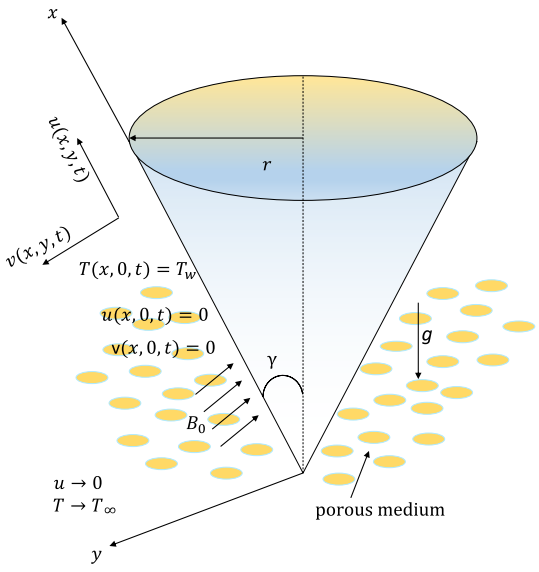


**Fig. 1** Graphical representation.

Here $r$ is the radius of the cone, $\rho$ is the density, $\tau_{xy}$ is the shear stress, $\mu$ is the dynamic viscosity, $k_0$ is the permeability, $\sigma$ is the electrical conductivity, $B_0$ refers to applied magnetic strength, $g$ is the gravitational acceleration, and $\beta_T$ is the thermal expansion, $T$ is the temperature, and the subscript $hnf$ refers to hybrid nanofluid. Furthermore, the mathematical expressions of $\rho_{hnf}, \mu_{hnf}, \sigma_{hnf}$ and $(\rho\beta_T)_{hnf}$ are provided by [13,14,18]:

$$\begin{aligned}\rho_{hnf} &= (1-\varphi_{s_2})\rho_{nf}+\varphi_{s_2}\rho_{s_2},\ \mu_{hnf}=\frac{\mu_f}{(1-\varphi_{s_1})^{2.5}(1-\varphi_{s_2})^{2.5}},\\ \frac{\sigma_{hnf}}{\sigma_{nf}} &= \frac{(\sigma_{s_2}+2\sigma_{nf})+2\varphi_{s_2}(\sigma_{s_2}-\sigma_{nf})}{(\sigma_{s_2}+2\sigma_{nf})-\varphi_{s_2}(\sigma_{s_2}-\sigma_{nf})},\ (\rho\beta_T)_{hnf}=(1-\varphi_{s_2})(\rho\beta_T)_{nf}+\varphi_{s_2}(\rho\beta_T)_{s_2}.\end{aligned} \tag{3}$$

The thermal and physical properties of water and nanoparticles are presented in Table 1. The stress component $\tau_{xy}$ is defined by the following relation [22]

$$(1+\lambda_1^\alpha\partial_t^\alpha)\tau_{xy}=\mu_{hnf}\frac{\partial u}{\partial y}, \tag{4}$$

where $\lambda_1$ denotes relaxation time, $\alpha$ is the fractional order, and $\partial_t^\alpha$ is the Caputo fractional derivative of order $\alpha$, defined as [31]

$$\begin{aligned}\partial_t^\alpha g(t) &= \frac{\partial^\alpha}{\partial t^\alpha}g(t)\\ &= \frac{1}{\Gamma(n-\alpha)}\int_0^t (t-s)^{n-\alpha-1}\frac{\partial^n}{\partial s^n}g(s)ds,\ \ n-1<\alpha\\ &< n,\ n\in\mathbf{N}.\end{aligned} \tag{5}$$

The Gamma function $\Gamma(\cdot)$ is

$$\Gamma(\xi)=\int_{\mathbf{R}}\eta^{\xi-1}e^{-\eta}d\eta,\ \forall\xi\in\mathbf{C},\ \Re(\xi)>0. \tag{6}$$

Evaluating $\tau_{xy}$ form Eqs. (2) and (4) leads us to

$$\begin{aligned}(1+\lambda_1^\alpha\partial_t^\alpha)\left(\frac{\partial u}{\partial t}+u\frac{\partial u}{\partial x}+v\frac{\partial u}{\partial y}\right) &= \nu_{hnf}\frac{\partial^2 u}{\partial y^2}-\frac{\nu_{hnf}}{k_0}(1+\lambda_1^\alpha\partial_t^\alpha)u-\frac{\sigma_{hnf}}{\rho_{hnf}}B_0^2(1+\lambda_1^\alpha\partial_t^\alpha)u\\ &+g\frac{(\rho\beta_T)_{hnf}}{\rho_{hnf}}(1+\lambda_1^\alpha\partial_t^\alpha)(T-T_\infty)\cos\gamma.\end{aligned} \tag{7}$$

Assuming that the effects of viscous dissipation are minimal, then the energy equation including thermal radiation is [36]

**Table 1** Thermo-physical properties of water nanoparticles [10,12].

| Materials | $\rho$ | $\sigma$ | $\beta_T$ | $C_p$ | $k$ |
|---|---|---|---|---|---|
| | $kgm^{-3}$ | $Sm^{-1}$ | $K^{-1}$ | $J(kgK)^{-1}$ | $W(mK)^{-1}$ |
| Pure water | 997.1 | 0.05 | $21\times10^{-5}$ | 4179 | 0.613 |
| $Fe_3O_4$ | 5200 | $2.5\times10^{4}$ | $1.3\times10^{-5}$ | 670 | 6 |
| Cu | 8933 | $5.96\times10^{7}$ | $1.67\times10^{-5}$ | 385 | 401 |

$$\left(\rho C_p\right)_{hnf}\left(\frac{\partial T}{\partial t}+u\frac{\partial T}{\partial x}+v\frac{\partial T}{\partial y}\right)=-\frac{\partial q}{\partial y}-\frac{\partial q_r}{\partial y}, \tag{8}$$

where $\left(\rho C_p\right)_{hnf}$ represents heat capacitance, $q$ is the heat flux, $q_r$ is radiative heat flux. The mathematical expressions of $\left(\rho C_p\right)_{hnf}$ and $k_{hnf}$ are given as [13]

$$\left(\rho C_p\right)_{hnf}=(1-\varphi_{s_2})\left(\rho C_p\right)_{nf}+\varphi_{s_2}\left(\rho C_p\right)_{s_2},\ \frac{k_{hnf}}{k_{nf}}=\frac{\left(k_{s_2}+2k_{nf}\right)+2\varphi_{s_2}\left(k_{s_2}-k_{nf}\right)}{\left(k_{s_2}+2k_{nf}\right)-\varphi_{s_2}\left(k_{s_2}-k_{nf}\right)}. \tag{9}$$

Furthermore, Rosseland approximation for $q_r$ is [31]

$$q_r=-\frac{4\sigma_b}{3k_b}\frac{\partial T^4}{\partial y}, \tag{10}$$

where $k_b$ and $\sigma_b$ denote the absorption and Stefan–Boltzmann coefficients, respectively. The temperature difference $T-T_\infty$ within the flow is assumed to be small. Consequently, the Taylor approximation for $T^4$ is (neglecting higher terms):

$$T^4=T_\infty^4+4T_\infty^3(T-T_\infty). \tag{11}$$

Moreover, the fractional Cattaneo heat flux [29,37] gives us

$$\left(1+\lambda_2^\beta\partial_t^\beta\right)q=-k_{hnf}\frac{\partial T}{\partial y}. \tag{12}$$

Using Eqs. (10)-(12), in Eq. (8) gives us

$$\left(\rho C_p\right)_{hnf}\left(1+\lambda_2^\beta\partial_t^\beta\right)\left(\frac{\partial T}{\partial t}+u\frac{\partial T}{\partial x}+v\frac{\partial T}{\partial y}\right)=\left(k_{hnf}+\frac{16\sigma_b}{3k_b}\right)\frac{\partial^2 T}{\partial y^2}. \tag{13}$$

The assumed initial and boundary conditions are

$$\begin{aligned}
&u(x,y,0)=0, \quad v(x,y,0)=0, \quad T(x,y,0)=T_\infty,\\
&u(0,y,t)=0, \qquad\qquad\quad T(0,y,t)=T_\infty,\\
&u(x,0,t)=0, \quad v(x,0,t)=0, \quad T(x>0,0,t)=T_w,\\
&u(x,\infty,t)=0, \qquad\qquad\quad T(x,\infty,t)=T_\infty.
\end{aligned} \tag{14}$$

## 3. Non-dimensional problem

Non-dimensional variables simplify the computing process by allowing units of variables to be discarded. Therefore, a set of non-dimensional parameters listed below are introduced [19]

$$\begin{aligned}
x^* &= \tfrac{x}{L}, & y^* &= \tfrac{y}{L}(Gr)^{\frac{1}{4}}, & t^* &= \tfrac{\nu_f t}{L^2}(Gr)^{\frac{1}{2}},\\
u^* &= \tfrac{uL}{\nu_f}(Gr)^{\frac{-1}{2}}, & v^* &= \tfrac{vL}{\nu_f}(Gr)^{\frac{-1}{4}}, & T^* &= \tfrac{T-T_\infty}{T_w-T_\infty},\\
Gr &= \tfrac{g\beta_T(T_w-T_\infty)L^3}{\nu_f^2}, & \lambda_1^* &= \tfrac{\nu_f\lambda_1}{L^2}(Gr)^{\frac{1}{2}}, & \lambda_2^* &= \tfrac{\nu_f\lambda_2}{L^2}(Gr)^{\frac{1}{2}}.
\end{aligned} \tag{15}$$

Using non-dimensional parameters (15) in Eqs. (1), (7), (13) and (14), we arrived at (removing the $*$):

$$\frac{\partial}{\partial x}(ru)+\frac{\partial}{\partial y}(rv)=0, \tag{16}$$

$$\begin{aligned}
&\mathscr{C}_1\left(1+\lambda_1^\alpha\frac{\partial^\alpha}{\partial t^\alpha}\right)\left(\frac{\partial u}{\partial t}+u\frac{\partial u}{\partial x}+v\frac{\partial u}{\partial y}\right)\\
&\quad=\mathscr{C}_2\frac{\partial^2 u}{\partial y^2}-\left(\frac{\mathscr{C}_2}{K}+\mathscr{C}_3 M\right)\left(1+\lambda_1^\alpha\frac{\partial^\alpha}{\partial t^\alpha}\right)u+\mathscr{C}_4\\
&\qquad\times\cos\gamma\left(1+\lambda_1^\alpha\frac{\partial^\alpha}{\partial t^\alpha}\right)T,
\end{aligned} \tag{17}$$

$$\mathscr{C}_5\left(1+\lambda_2^\beta\frac{\partial^\beta}{\partial t^\beta}\right)\left(\frac{\partial T}{\partial t}+u\frac{\partial T}{\partial x}+v\frac{\partial T}{\partial y}\right)=\frac{\mathscr{C}_6+Rd}{Pr}\frac{\partial^2 T}{\partial y^2}. \tag{18}$$

subject to initial boundary conditions:

$$\begin{aligned}
&u(x,y,0)=0, \quad v(x,y,0)=0, \quad T(x,y,0)=0,\\
&u(0,y,t)=0, \qquad\qquad\quad T(0,y,t)=0,\\
&u(x,0,t)=0, \quad v(x,0,t)=0, \quad T(x>0,0,t)=1,\\
&u(x,\infty,t)=0, \qquad\qquad\quad T(x,\infty,t)=0.
\end{aligned} \tag{19}$$

The nanofluid constants $\mathscr{C}_1-\mathscr{C}_6$ represent nanofluid constant coefficients defined as

$$\begin{aligned}
&Pr=\tfrac{\left(\mu C_p\right)_f}{k_f},\ \tfrac{1}{K}=\tfrac{L^2}{k_0}(Gr)^{\frac{1}{2}},\ M=\tfrac{\sigma_f B_0^2 L^2}{\mu_f}(Gr)^{\frac{1}{2}},\ Rd=\tfrac{16\sigma_b T_\infty^{\,3}}{3k_b k_f},\\
&\mathscr{C}_1=(1-\varphi_{s_2})\tfrac{\rho_{nf}}{\rho_f}-\varphi\tfrac{\rho_{s_2}}{\rho_f},\ \mathscr{C}_2=\left((1-\varphi_{s_1})(1-\varphi_{s_2})\right)^{-2.5},\ \mathscr{C}_3=\tfrac{\sigma_{hnf}}{\sigma_f},\\
&\mathscr{C}_4=(1-\varphi_{s_2})\tfrac{(\rho\beta_T)_{nf}}{(\rho\beta_T)_f}-\varphi\tfrac{(\rho\beta_T)_{s_2}}{(\rho\beta_T)_f},\ \mathscr{C}_5=(1-\varphi_{s_2})\tfrac{\left(\rho C_p\right)_{nf}}{\left(\rho C_p\right)_f}-\varphi\tfrac{\left(\rho C_p\right)_{s_2}}{\left(\rho C_p\right)_f},\ \mathscr{C}_6=\tfrac{k_{hnf}}{k_f}.
\end{aligned} \tag{20}$$

## 4. Physical quantities

The wall shear stress $\tau_w$ and Nusselt number $Nu_x$ for the Maxwell fluid can be evaluate by following relations [22]

$$\left(1+\lambda_1^{\alpha}\partial_t^{\alpha}\right)\tau_w = \mu_{hnf}\frac{\partial u}{\partial y}_{y=0}, \quad \left(1+\lambda_2^{\beta}\partial_t^{\beta}\right)Nu_x = \frac{k_{hnf}x}{k_f(T_w-T_\infty)}\left(\frac{\partial T}{\partial y}\right)_{y=0}. \tag{21}$$

The following non-dimensional forms are obtained using parameters (15)

$$\left(1+\lambda_1^{\alpha}\partial_t^{\alpha}\right)\tau_W Gr^{-3/4} = \mathscr{C}_2\left(\frac{\partial u}{\partial y}\right)_{y=0}, \quad \left(1+\lambda_2^{\beta}\partial_t^{\beta}\right)Nu_x Gr^{1/4} = \mathscr{C}_6 x\left(\frac{\partial T}{\partial y}\right)_{y=0}, \tag{22}$$

where $\tau_W = \frac{\tau_w L^2}{\nu_f \mu_f}$.

## 5. Numerical procedure

The Crank-Nicolson approach is used to approximate the integer-order derivatives and L1 algorithm of Caputo derivatice is used to evaluate the fraction order derivatives of nonlinear, coupled, partial differential Eqs. (16)-(18). If $\left(w_{1_{i,j}}^k, w_{2_{i,j}}^k\right)$ are the numerical solutions at $(x_i, y_j, t_k)$ with time step $\Delta t$ and mesh size $(\Delta x, \Delta y)$ such that $t_k = k\Delta t, k = 0, 1, \cdots, n$ $x_i = i\Delta x, i = 1, 2, \cdots, p$ and $y_j = j\Delta y, j = 1, 2, \cdots, q$, then the derivatives can be approximated as follows [23]:

1. Integer-order derivatives using Crank-Nicolson method:

$$\frac{\partial w_1}{\partial t}(x,y,t) \simeq \frac{\partial w_1}{\partial t}(x_i,y_j,t_{k+1}) \simeq \frac{w_{1_{i,j}}^{k+1} - w_{1_{i,j}}^{k}}{\Delta t}. \tag{23}$$

$$w_1\frac{\partial w_1}{\partial x}(x,y,t) \simeq w_1\frac{\partial w_1}{\partial x}(x_i,y_j,t_{k+1}) \simeq w_{1_{i,j}}^{k}\frac{w_{1_{i,j}}^{k+1} - w_{1_{i-1,j}}^{k+1} + w_{1_{i,j}}^{k} - w_{1_{i-1,j}}^{k}}{2\Delta x}. \tag{24}$$

$$w_2\frac{\partial w_1}{\partial y}(x,y,t) \simeq w_2\frac{\partial w_1}{\partial y}(x_i,y_j,t_{k+1}) \simeq w_{2_{i,j}}^{k}\frac{w_{1_{i,j+1}}^{k+1} - w_{1_{i,j-1}}^{k+1} + w_{1_{i,j+1}}^{k} - w_{1_{i,j-1}}^{k}}{4\Delta y}. \tag{25}$$

$$\frac{\partial^2 w_1}{\partial y^2}(x,y,t) \simeq \frac{\partial^2 w_1}{\partial y^2}(x_i,y_j,t_{k+1}) \simeq \frac{w_{1_{i,j+1}}^{k+1} - 2w_{1_{i,j}}^{k+1} + w_{1_{i,j-1}}^{k+1} + w_{1_{i,j+1}}^{k} - 2w_{1_{i,j}}^{k} + w_{1_{i,j-1}}^{k}}{2\Delta y^2}. \tag{26}$$

2. fractional order derivative using L1 algorithm and Crank-Nicolson method:

$$\frac{\partial^{\alpha} w_1}{\partial t^{\alpha}} \simeq \frac{\Delta t^{-\alpha}}{2\Gamma(2-\alpha)}\left[w_{1_{i,j}}^{k+1} + w_{1_{i,j}}^{k} + \sum_{m=1}^{k} b_m w_{1_{i,j}}^{k+1-m} + \sum_{m=1}^{k-1} b_m w_{1_{i,j}}^{k-m}\right], \tag{27}$$

where $b_m = (a_m - a_{m-1}),\ a_m = (m+1)^{1-\alpha} - m^{1-\alpha}$.

Using . Eqs. (23)-(27) in Eqs. (16)-(18) results in the systems of linear equations which have been further solved in MATLAB software. The time-step $\Delta t$ and mesh sizes $(\Delta x, \Delta y)$ are taekn as: $\Delta t = 0.001, \Delta x = 0.05$, and $\Delta y = 0.05$. Following some preliminary investigation, $y_{max}$ is determined to be 9, which is far distant from the momentum and temperature boundary layers.

## 6. Analysis of resutls

This section is intended to aid comprehension of explanation of graphical depictions and discuss the theoretical aspects of problem, including the Cu-$Fe_3O_4$ volume concentration, relation parameter, thermal radiation parameter, magnetic parameter, porosity parameter, and fractional-order derivative.

### 6.1. Temperature and velocity profiles

The purpose of Figs. 2–9, is to assess the influence of all controlling factors/parameter on Maxwell fluid characteristics. The influence of fractional parameter $\alpha$ on velocity patterns has shown in Fig. 2. This figure reveals that the velocity profiles exhibit an decreasing tendency at the beginning level and a increasing trend with higher fractional parameter values. Physically, this is due to the fact that higher values of the fractional parameter create resistance in the flow of maxwell hybrid nanofluid, and thus the momentum of the fluid decreases. Moreover, as $\alpha$ increases, the thickness of momentum boundary layers decreases, consequently the velocity profile declines prior to $y = 0.7$. Fig. 3 displays an increase in the velocity field as the relaxation parameter $\lambda_1$ is enlarged. As $\lambda_1$ increases, the velocity field widens, which increases the time necessary to return to a normal condition. This can be physically explained as the time required for momentum flow to occur after the velocity gradient is formed. Fig. 4 illustrates the impact of $\varphi$ on velocity profiles. The velocity of hybrid nanofluids decreases as the nanoparticle volume percentage increases. This is physically plausible since the viscosity of the hybrid nanofluid increased as $\varphi$ increased, resulting in a reduction in the nanofluid velocity and thickness of momentum barrier layer. In Fig. 5, the properties of velocity profiles in the presence of the porosity parameter $K$ for Maxwell hybrid nanofluid are illustrated. A increase in velocity profiles is caused by rising $K$ values. This is plausible since a porous media offers fluid flow without resistance. Consequently, as seen in Fig. 5, large values of the $K$ parameter increase fluid velocity and momentum thickness of layer. The influence of the magnetic parameter $M$ on the velocity profiles of Maxwell hybrid nanofluids is seen in Fig. 6. As the anticipated value of $M$ increases, the velocity of nanofluids drops. Because an increase in $M$ indicates an improvement in resistive force (the Lorentz force), the velocity of the Maxwell hybrid nanofluid is decreased. The influence of the fractional parameter $\beta$ on the temperature profiles is seen in Fig. 7. The temperature profiles exhibit an upward tendency for changes in the fractional parameter $\beta$. For longer durations, the temperature profiles showed an increasing trend for higher values of $\beta$. When $\beta$ is raised, the thickness of thermal boundary layers increases, reaching a maximum at $\beta = 0.9$, which correlates to a rise in

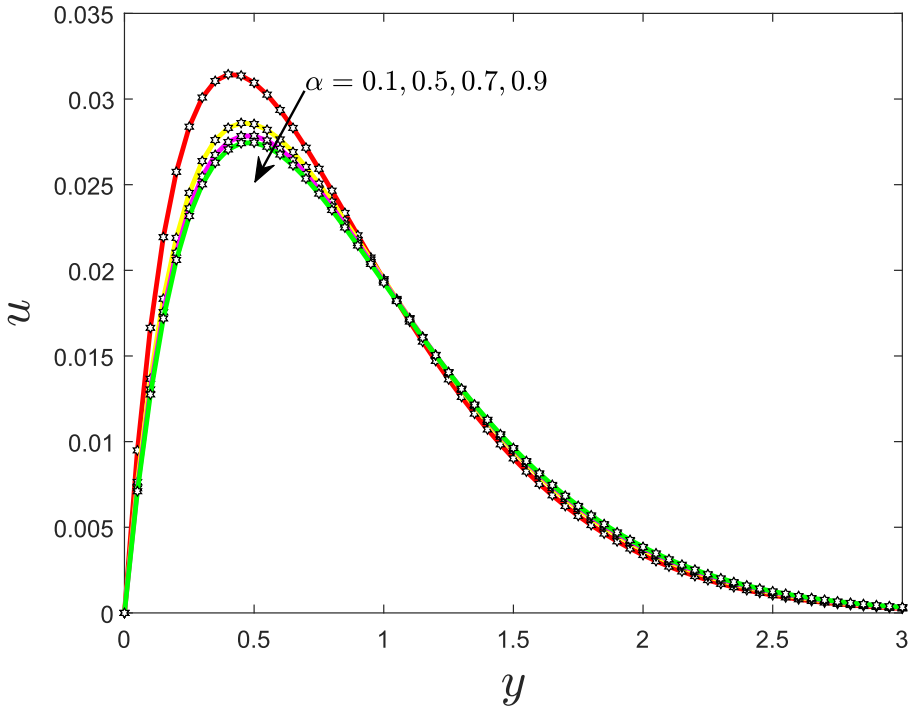


**Fig. 2** Effect of $\alpha$ on velocity field.

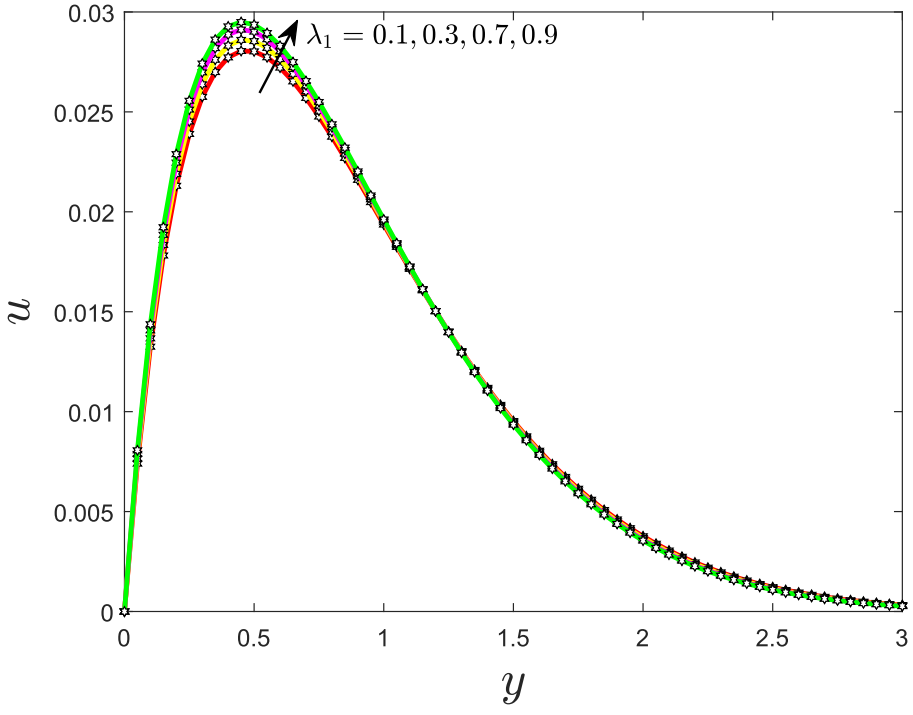


**Fig. 3** Effect of $\lambda_1$ on velocity field.

temperature profile performance. However, this impact reverses for a shorter duration when fractional temperature distributions are present. Fig. 8 demonstrates a drop in the temperature profiles when the relaxation parameter $\lambda_2$ is expanded. Physically, this is due to the fact that for large values of $\lambda_2$, the time required for heat flow to occur after the temperature gradient is formed, therefore, the temperature profile becomes smother. Fig. 9 depicts the variations in the temperature profile in relation to the radiation parameter *Rd* for Maxwell hybrid nanofluids. It is believed that an increase in *Rd* factor causes a rise in temperature. Physically, the *Rd* factor compares the input of heat exchange by conduction to thermal

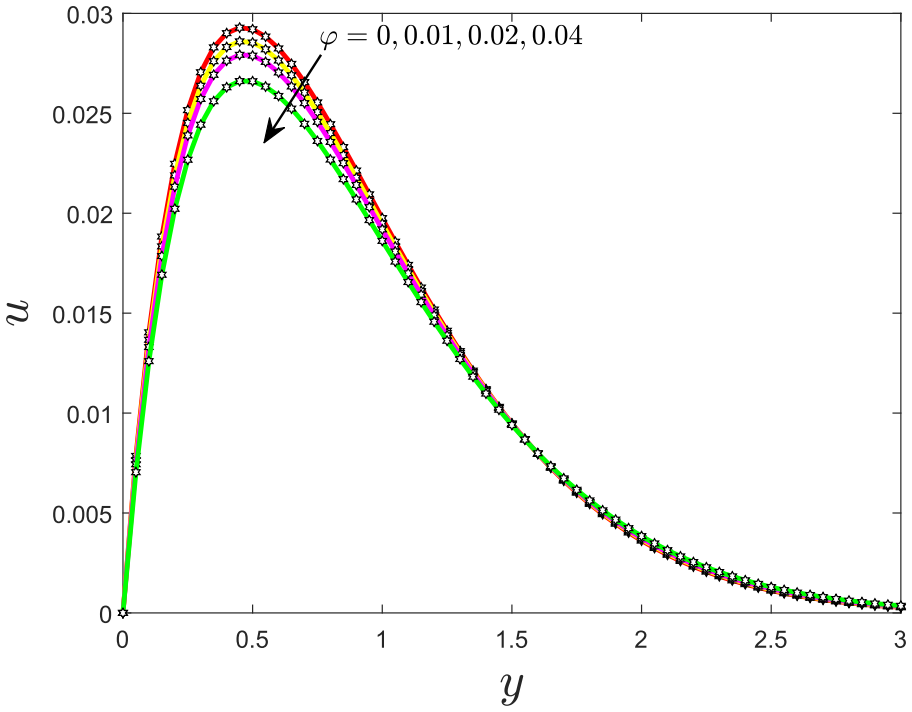


**Fig. 4** Effect of $\varphi$ on velocity field.

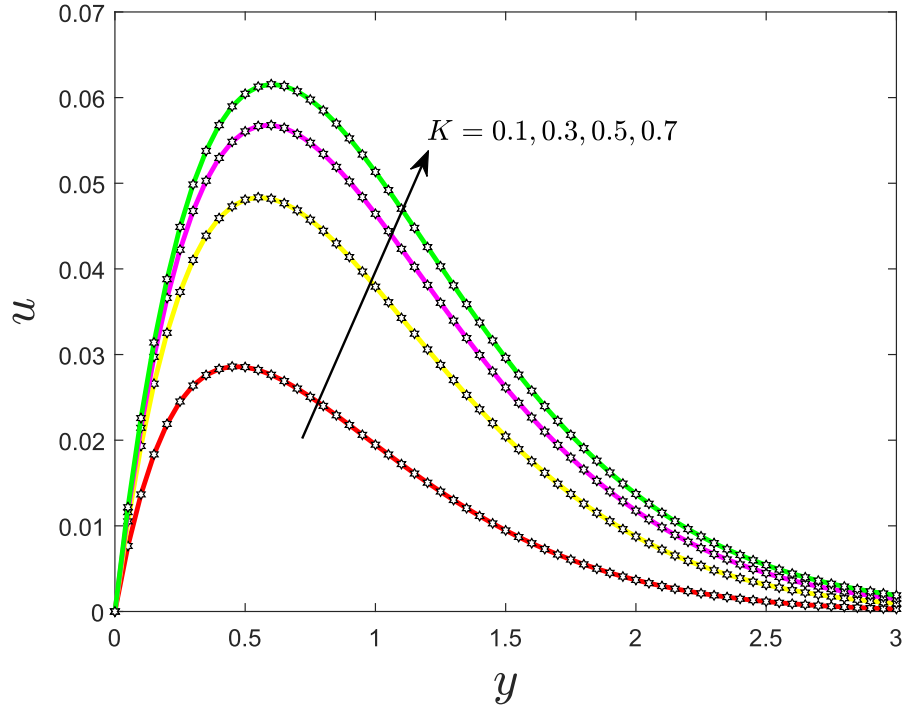


**Fig. 5** Effect of $K$ on velocity field.

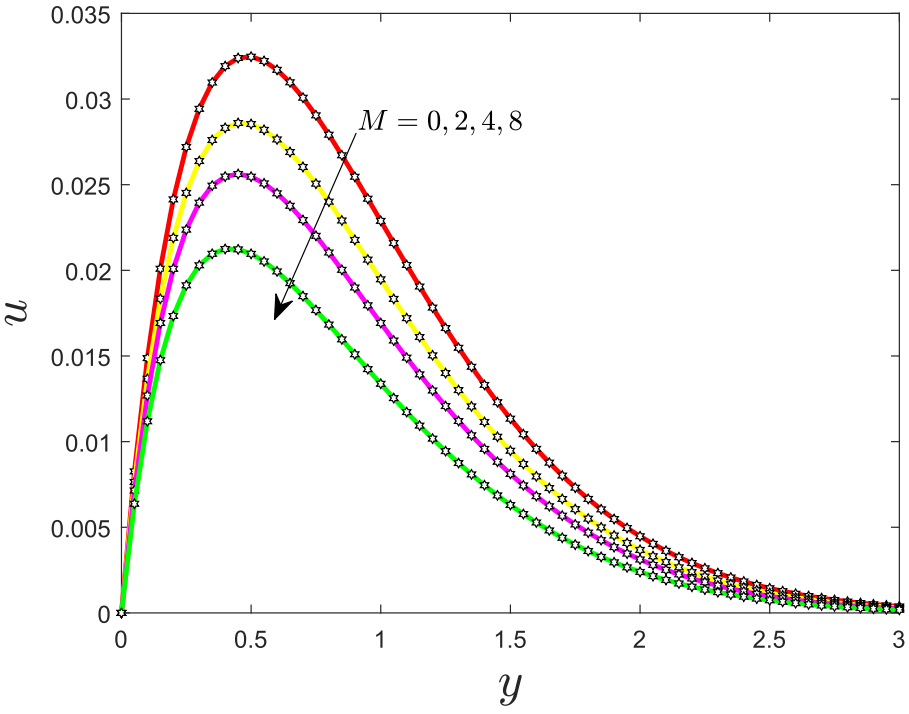


**Fig. 6** Effect of $M$ on velocity field.

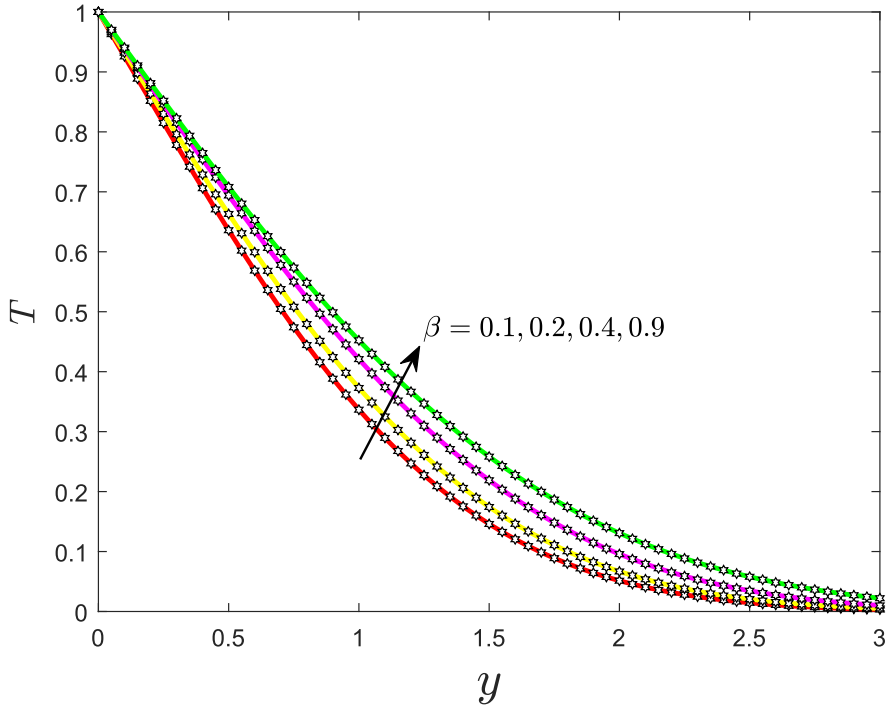


**Fig. 7** Effect of $\beta$ on temperature distribution.

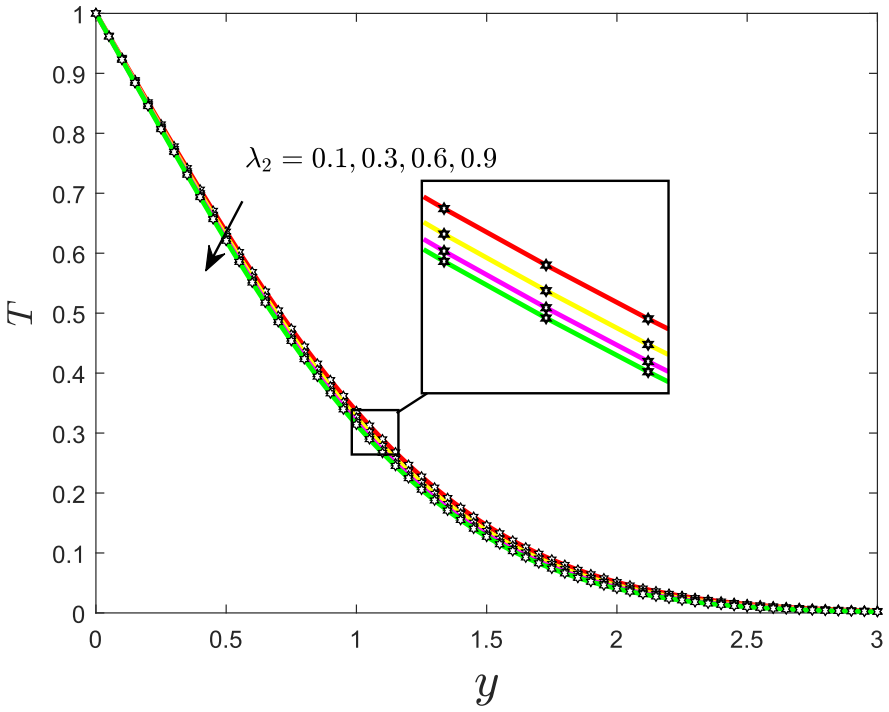


**Fig. 8** Effect of $\lambda_2$ on temperature distribution.

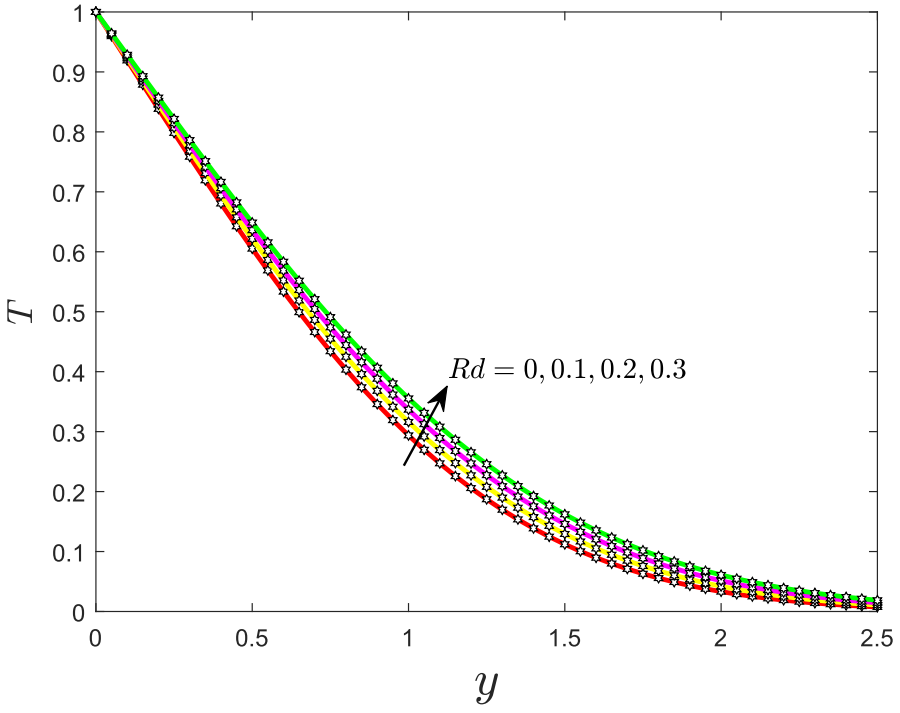


**Fig. 9** Effect of *Rd* on temperature distribution.

radiation transmission. Clearly, an increase in the radiation parameter induces a rise in temperature. In addition, there is a positive relationship between the *Rd* and the temperature gradient at the plate's surface. Consequently, the hybrid nanofluid has superior properties compared to the viscous fluid.

### *6.2. Physical quantities*

The effects of porosity parameter with magnetic number and velocity fractional derivative with time relaxation parameter on wall shear stress are shown in Figs. 10 and 11, respectively. It is easy to see that velocity gradients decrease with rising time

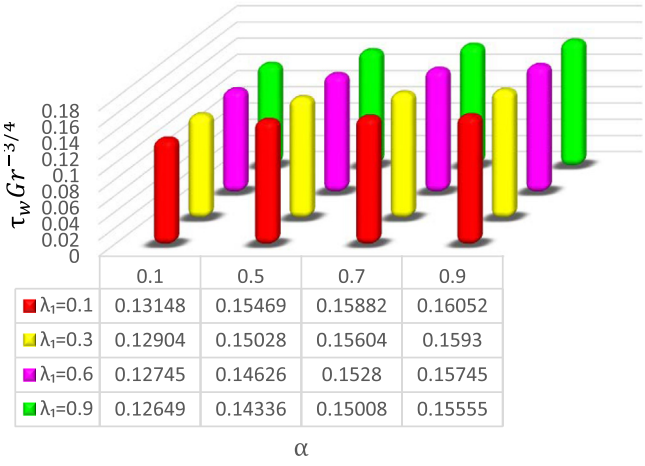


| | 0.1 | 0.5 | 0.7 | 0.9 |
|---|---|---|---|---|
| λ₁=0.1 | 0.13148 | 0.15469 | 0.15882 | 0.16052 |
| λ₁=0.3 | 0.12904 | 0.15028 | 0.15604 | 0.1593 |
| λ₁=0.6 | 0.12745 | 0.14626 | 0.1528 | 0.15745 |
| λ₁=0.9 | 0.12649 | 0.14336 | 0.15008 | 0.15555 |

**Fig. 10** Wall shear stress for distinct values of $\alpha$ and $\lambda_1$.

relaxation parameter and magnetic number but rise with increasing the fractional derivative and the porosity parameter. Figs. 12 and 13 depict the effects of the temperature fractional derivative with the temperature time relaxation parameter and the volume fraction parameter with the thermal radiation parameter on the Nusselt number, respectively. It is easy to see that increasing temperature time relaxation with constant and temperature fractional derivative decreases thermal gradient, whereas increasing temperature fractional derivative parameter with constant time relaxation increases thermal gradient. Thermal radiation with a volume fraction parameter exhibits the same Nusselt number behavior.

### 6.3. Particular cases

Tables 2–4, present specific numerical results for the various cases of the considered problems in the hope that other researchers and scientists working experimentally in this

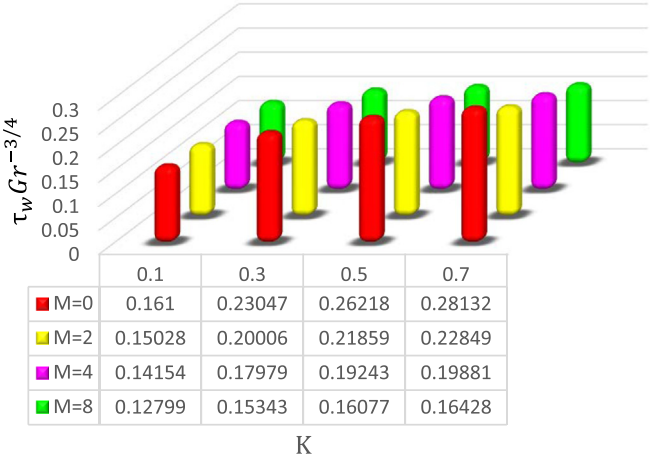


| | 0.1 | 0.3 | 0.5 | 0.7 |
|---|---|---|---|---|
| M=0 | 0.161 | 0.23047 | 0.26218 | 0.28132 |
| M=2 | 0.15028 | 0.20006 | 0.21859 | 0.22849 |
| M=4 | 0.14154 | 0.17979 | 0.19243 | 0.19881 |
| M=8 | 0.12799 | 0.15343 | 0.16077 | 0.16428 |

**Fig. 11** Wall shear stress for distinct values of $K$ and $M$.

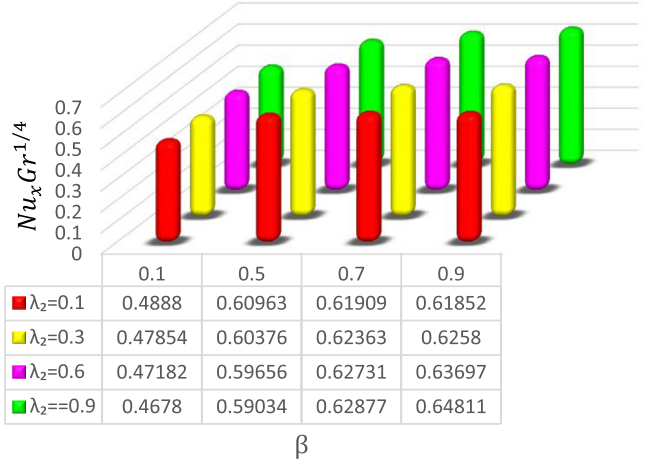


| | 0.1 | 0.5 | 0.7 | 0.9 |
|---|---|---|---|---|
| λ₂=0.1 | 0.4888 | 0.60963 | 0.61909 | 0.61852 |
| λ₂=0.3 | 0.47854 | 0.60376 | 0.62363 | 0.6258 |
| λ₂=0.6 | 0.47182 | 0.59656 | 0.62731 | 0.63697 |
| λ₂==0.9 | 0.4678 | 0.59034 | 0.62877 | 0.64811 |

**Fig. 12** Nusselt number for distinct values of $\beta$ and $\lambda_2$.

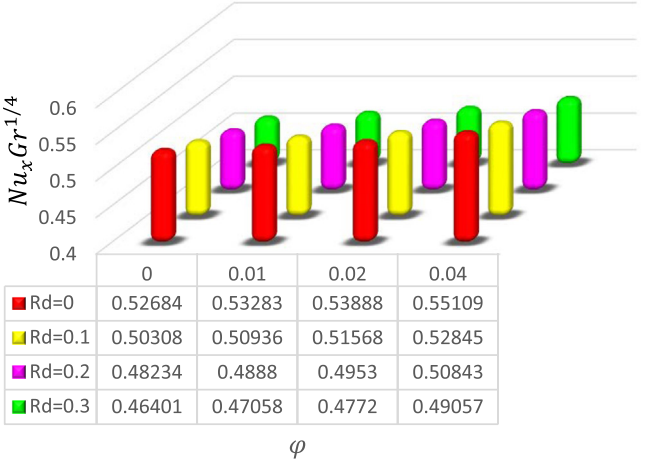


| | 0 | 0.01 | 0.02 | 0.04 |
|---|---|---|---|---|
| Rd=0 | 0.52684 | 0.53283 | 0.53888 | 0.55109 |
| Rd=0.1 | 0.50308 | 0.50936 | 0.51568 | 0.52845 |
| Rd=0.2 | 0.48234 | 0.4888 | 0.4953 | 0.50843 |
| Rd=0.3 | 0.46401 | 0.47058 | 0.4772 | 0.49057 |

**Fig. 13** Nusselt number for distinct values of $\varphi$ and $Rd$.

**Table 2** Shear stress and Nusselt number for Maxwell fluid when $M = 0$.

| $\alpha$ | $\lambda_1$ | $\beta$ | $\lambda_2$ | $k$ | $Rd$ | $\tau_W Gr^{-3/4}$ | $Nu_x Gr^{1/4}$ |
|---|---|---|---|---|---|---|---|
| 0.1 | 0.3 | 0.1 | 0.1 | 0.1 | 0.2 | 0.13911 | 0.48832 |
| 0.5 | | | | | | 0.16128 | 0.48507 |
| 0.7 | | | | | | 0.16731 | 0.48412 |
| 0.9 | | | | | | 0.17074 | 0.48351 |
| 0.5 | 0.1 | | | | | 0.16594 | 0.48423 |
| | 0.6 | | | | | 0.15704 | 0.48583 |
| | 0.9 | | | | | 0.15398 | 0.48639 |
| | 0.3 | 0.5 | | | | 0.16435 | 0.53283 |
| | | 0.7 | | | | 0.16794 | 0.59185 |
| | | 0.9 | | | | 0.16987 | 0.61516 |
| | | 0.1 | 0.3 | | | 0.16044 | 0.4748 |
| | | | 0.6 | | | 0.15987 | 0.46807 |
| | | | 0.9 | | | 0.15953 | 0.46405 |
| | | | 0.1 | 0.3 | | 0.2304 | 0.50671 |
| | | | | 0.5 | | 0.26179 | 0.51927 |
| | | | | 0.7 | | 0.28069 | 0.5279 |
| | | | | 0.1 | 0 | 0.15769 | 0.52952 |
| | | | | | 0.1 | 0.15959 | 0.50579 |
| | | | | | 0.3 | 0.1628 | 0.46676 |

**Table 3** Shear stress and Nusselt number for Maxwell fluid when $Rd = 0$.

| $\alpha$ | $\lambda_1$ | $\beta$ | $\lambda_2$ | $k$ | $M$ | $\tau_W Gr^{-3/4}$ | $Nu_x Gr^{1/4}$ |
|---|---|---|---|---|---|---|---|
| 0.1 | 0.3 | 0.1 | 0.1 | 0.1 | 2 | 0.12721 | 0.52976 |
| 0.5 | | | | | | 0.14752 | 0.52684 |
| 0.7 | | | | | | 0.15304 | 0.52598 |
| 0.9 | | | | | | 0.15619 | 0.52544 |
| 0.5 | 0.1 | | | | | 0.15179 | 0.52609 |
| | 0.6 | | | | | 0.14363 | 0.52752 |
| | 0.9 | | | | | 0.14083 | 0.52802 |
| | 0.3 | 0.5 | | | | 0.15033 | 0.57854 |
| | | 0.7 | | | | 0.15361 | 0.64224 |
| | | 0.9 | | | | 0.15535 | 0.66684 |
| | | 0.1 | 0.3 | | | 0.14676 | 0.51577 |
| | | | 0.6 | | | 0.14624 | 0.50852 |
| | | | 0.9 | | | 0.14592 | 0.50419 |
| | | | 0.1 | 0.3 | | 0.1946 | 0.54043 |
| | | | | 0.5 | | 0.2119 | 0.54622 |
| | | | | 0.7 | | 0.22109 | 0.5495 |
| | | | | 0.1 | 0 | 0.15769 | 0.52952 |
| | | | | | 4 | 0.1392 | 0.52474 |
| | | | | | 8 | 0.12622 | 0.52166 |

**Table 4** Shear stress and Nusselt number for Newtonian fluid.

| $k$ | $M$ | $Rd$ | $\tau_W Gr^{-3/4}$ | $Nu_x Gr^{1/4}$ |
|---|---|---|---|---|
| 0.1 | 2 | 0.2 | 0.16948 | 0.60449 |
| 0.3 | | | 0.22927 | 0.62647 |
| 0.5 | | | 0.25197 | 0.63641 |
| 0.7 | | | 0.26418 | 0.64218 |
| 0.1 | 0 | | 0.18213 | 0.60867 |
| | 4 | | 0.15923 | 0.60128 |
| | 8 | | 0.14343 | 0.59665 |
| | 2 | 0 | 0.16659 | 0.6602 |
| | | 0.1 | 0.16812 | 0.63047 |
| | | 0.3 | 0.17069 | 0.58154 |

domain of research will compare their results in order to validate their experimental results. Furthermore, if they achieve similar results to ours, the cost of the experiments can be reduced.

## 7. Conclusions

This study evaluates the influence of Cu-$Fe_3O_4$ nanomaterials, thermal radiation, and fractional derivatives on the flow and heat transmission properties of Maxwell Hybrid nanofluid. Using the Caputo derivative and Crank-Nicolson approach, the fractional Maxwell hybrid nanofluid model is solved. The outcomes of many relevant factors are examined numerically via graphs and physically discussed. The following are the key points obtained from this study:

- The velocity (temperature) profiles demonstrate that for rising values of $\alpha(\beta)$, the diminishing (increasing) behavior is most pronounced $\alpha = 0.9(\beta = 0.9)$ over a longer period of time.
- The velocity (temperature) profiles demonstrate an increasing (decreasing) trend for rising $\lambda_1(\lambda_2)$ values.
- The velocity profiles decrease when the magnetic and volume fraction parameters are increased.
- The velocity profile reduced by increasing the intensity of the magnetic field.
- The thickness of the thermal boundary layer increases when the radiation parameter is increased.
- When the volume fraction parameter value is small (large), the velocity increases (decreases).

## Declaration of Competing Interest

The authors declare that they have no known competing financial interests or personal relationships that could have appeared to influence the work reported in this paper.

## Acknowledgment

The authors would like to acknowledge the financial support from Universiti Teknologi Malaysia for the funding under UTM High Impact Research (UTMHR: Q. J130000.2454.08G33).

## References

[1] S.U. Choi, J.A. Eastman, Enhancing thermal conductivity of fluids with nanoparticles, Technical Report, Argonne National Lab. (ANL), Argonne, IL (United States), 1995.
[2] J. Buongiorno, Convective transport in nanofluids, AsME J. Heat Transf. (2006), https://doi.org/10.1115/1.2150834.
[3] R. Mahat, M. Saqib, I. Khan, S. Shafie, N.A.M. Noor, Thermal radiation effect on viscoelastic walters'-B nanofluid flow through a circular cylinder in convective and constant heat flux, Case Stud. Therm. Eng. 39 (2022) 102394, https://doi.org/10.1016/j.csite.2022.102394.
[4] N.A. Mat Noor, S. Shafie, M.A. Admon, Slip effects on MHD squeezing flow of Jeffrey nanofluid in horizontal channel with chemical reaction, Mathematics 9 (2021) 1215, https://doi.org/10.3390/math9111215.
[5] M.I. Asjad, N. Sarwar, B. Ali, S. Hussain, T. Sitthiwirattham, J. Reunsumrit, Impact of bioconvection and chemical reaction on MHD nanofluid flow due to exponential stretching sheet, Symmetry 13 (2021) 2334, https://doi.org/10.3390/sym13122334.
[6] H. Hanif, A finite difference method to analyze heat and mass transfer in kerosene based $\gamma$-oxide nanofluid for cooling applications, Phys. Scr. 96 (2021) 095215, https://doi.org/10.1088/1402-4896/ac098a.
[7] S. Ghasemi, M. Hatami, Solar radiation effects on MHD stagnation point flow and heat transfer of a nanofluid over a stretching sheet, Case Stud. Therm. Eng. 25 (2021) 100898, https://doi.org/10.1016/j.csite.2021.100898.
[8] R. Mahat, M. Saqib, I. Ulah, S. Shafie, S.M. Isa, Magnetohydrodynamics mixed convection of viscoelastic nanofluid past a circular cylinder with constant heat flux, CFD Lett. 14 (2022) 52–59,, https://doi.org/10.37934/cfdl.14.9.5259.
[9] U. Mahabaleshwar, K. Sneha, H.-N. Huang, An effect of MHD and radiation on CNTS-water based nanofluids due to a stretching sheet in a newtonian fluid, Case Stud. Therm. Eng. 28 (2021) 101462, https://doi.org/10.1016/j.csite.2021.101462.
[10] H. Hanif, S. Shafie, N.A. Rawi, A.R.M. Kasim, Entropy analysis of magnetized ferrofluid over a vertical flat surface with variable heating, Alexandria Eng. J. 65 (2023) 897–908, https://doi.org/10.1016/j.aej.2022.09.052.
[11] N. Santhosh, R. Sivaraj, V. Ramachandra Prasad, O. Anwar Bég, H.-H. Leung, F. Kamalov, S. Kuharat, Computational study of MHD mixed convective flow of cu/$Al_2O_3$-water nanofluid in a porous rectangular cavity with slits, viscous heating, joule dissipation and heat source/sink effects, Waves in Random and Complex Media (2023) 1–34, https://doi.org/10.1080/17455030.2023.2168786.
[12] K. Thirumalaisamy, S. Ramachandran, V. Ramachandra Prasad, O. Anwar Bég, H.-H. Leung, F. Kamalov, R. Panneer Selvam, Comparative heat transfer analysis of electroconductive $Fe_3O_4$–MWCNT–water and $Fe_3O_4$–MWCNT–kerosene hybrid nanofluids in a square porous cavity using the non-Fourier heat flux model, Phys. Fluids 34 (2022) 122016, https://doi.org/10.1063/5.0127463.
[13] H. Hanif, I. Khan, S. Shafie, A novel study on time-dependent viscosity model of magneto-hybrid nanofluid flow over a permeable cone: Applications in material engineering, Eur. Phys. J. Plus 135 (2020) 730, https://doi.org/10.1140/epjp/s13360-020-00724-x.
[14] H. Hanif, I. Khan, S. Shafie, A novel study on hybrid model of radiative Cu–$Fe_3O_4$/water nanofluid over a cone with PHF/PWT, Eur. Phys. J. Special Top. 230 (2021) 1257–1271, https://doi.org/10.1140/epjs/s11734-021-00042-y.
[15] M.K.A. Mohamed, H.R. Ong, H.T. Alkasasbeh, M.Z. Salleh, Heat transfer of ag-Al2O3/water hybrid nanofluid on a stagnation point flow over a stretching sheet with newtonian heating, in: Journal of Physics: Conference Series, IOP Publishing, p. 042085. https://doi.org/10.1088/1742-6596/1529/4/042085.
[16] M. Ramzan, S. Riasat, S.F. Aljurbua, H.A.S. Ghazwani, O. Mahmoud, Hybrid nanofluid flow induced by an oscillating disk considering surface catalyzed reaction and nanoparticles shape factor, Nanomaterials 12 (2022) 1794, https://doi.org/10.3390/nano12111794.
[17] D. Gamachu, W. Ibrahim, Mixed convection flow of viscoelastic ag-$Al_2O_3$/water hybrid nanofluid past a rotating disk, Phys. Scr. 96 (2021) 125205, https://doi.org/10.1088/1402-4896/ac1a89.
[18] N.A. Shah, I. Animasaun, A. Wakif, O. Koriko, R. Sivaraj, K. Adegbie, Z. Abdelmalek, H. Vaidyaa, A. Ijirimoye, K. Prasad, Significance of suction and dual stretching on the dynamics of various hybrid nanofluids: Comparative analysis between type i and type ii models, Phys. Scr. 95 (2020) 095205, https://doi.org/10.1088/1402-4896/aba8c6.

[19] H. Hanif, I. Khan, S. Shafie, Heat transfer exaggeration and entropy analysis in magneto-hybrid nanofluid flow over a vertical cone: a numerical study, J. Therm. Anal. Calorim. 141 (2020) 2001–2017, https://doi.org/10.1007/s10973-020-09256-z.
[20] P. Vijayalakshmi, R. Sivaraj, Numerical simulation of hybrid nanofluid (cu/$Al_2O_3$-water) flow in a porous enclosure with heated corners and non-fourier heat flux, Proc. Inst. Mech. Eng., Part E: J. Process Mech. Eng. (2022), https://doi.org/10.1177/09544089221122063, 09544089221122063.
[21] K. Thirumalaisamy, S. Ramachandran, Comparative heat transfer analysis on $Fe_3O_4$–$H_2O$ and $Fe_3O_4$–Cu–$H_2O$ flow inside a tilted square porous cavity with shape effects, Phys. Fluids 35 (2023) 022007, https://doi.org/10.1063/5.0136326.
[22] H. Hanif, Cattaneo-Friedrich and Crank-Nicolson analysis of upper-convected Maxwell fluid along a vertical plate, Chaos, Solitons & Fractals 153 (2021) 111463, https://doi.org/10.1016/j.chaos.2021.111463.
[23] H. Hanif, A computational approach for boundary layer flow and heat transfer of fractional maxwell fluid, Math. Comput. Simul. 191 (2022) 1–13, https://doi.org/10.1016/j.matcom.2021.07.024.
[24] D. Vieru, C. Fetecau, N.A. Shah, S.-J. Yook, Unsteady natural convection flow due to fractional thermal transport and symmetric heat source/sink, Alexandria Eng. J. 64 (2023) 761–770, https://doi.org/10.1016/j.aej.2022.09.027.
[25] M. Saqib, H. Hanif, T. Abdeljawad, I. Khan, S. Shafie, K.S. Nisar, Heat transfer in MHD flow of Maxwell fluid via fractional Cattaneo-Friedrich model: A finite difference approach, Comput. Mater. Contin 65 (2020) 1959–1973, https://doi.org/10.32604/cmc.2020.011339.
[26] M. Al Nuwairan, A. Hafeez, A. Khalid, B. Souayeh, N. Alfadhli, A. Alnaghmosh, Flow of Maxwell fluid with heat transfer through porous medium with thermophoresis particle deposition and Soret-Dufour effects, Numerical solution, Coatings 12 (2022) 1567, https://doi.org/10.3390/coatings12101567.
[27] C. Fetecau, R. Ellahi, S.M. Sait, Mathematical analysis of Maxwell fluid flow through a porous plate channel induced by a constantly accelerating or oscillating wall, Mathematics 9 (2021) 90, https://doi.org/10.3390/math9010090.
[28] K. Loganathan, N. Alessa, N. Namgyel, T. Karthik, MHD flow of thermally radiative Maxwell fluid past a heated stretching sheet with cattaneo–christov dual diffusion, J. Math. 2021 (2021) 1–10, https://doi.org/10.1155/2021/5562667.
[29] K.Z. Zhang, N.A. Shah, D. Vieru, E.R. El-Zahar, Memory effects on conjugate buoyant convective transport of nanofluids in annular geometry: A generalized Cattaneo law of thermal flux, Int. Commun. Heat Mass Transfer 135 (2022) 106138, https://doi.org/10.1016/j.icheatmasstransfer.2022.106138.
[30] N. Sadiq, M. Imran, C. Fetecau, N. Ahmed, Rotational motion of fractional Maxwell fluids in a circular duct due to a time-dependent couple, Boundary Value Problems 2019 (2019) 1–11, https://doi.org/10.1186/s13661-019-1132-1.
[31] H. Hanif, S. Shafie, Impact of $Al_2O_3$ in electrically conducting mineral oil-based Maxwell nanofluid: Application to the petroleum industry, Fractal and Fractional 6 (2022) 180, https://doi.org/10.3390/fractalfract6040180.
[32] H. Hanif, S. Shafie, Interaction of multi-walled carbon nanotubes in mineral oil based Maxwell nanofluid, Scient. Rep. 12 (2022) 1–16, https://doi.org/10.1038/s41598-022-07958-y.
[33] Y. Zhang, J. Gao, Y. Bai, Q. Wang, D. Sun, X. Sun, B. Lv, Numerical simulation of the fractional Maxwell fluid flow in locally narrow artery, Comput. Methods Biomech. Biomed. Eng. (2022) 1–16, https://doi.org/10.1080/10255842.2022.2113781.
[34] H. Hanif, S. Shafie, Application of Cattaneo heat flux to Maxwell hybrid nanofluid model: a numerical approach, Eur. Phys. J. Plus 137 (2022) 989, https://doi.org/10.1140/epjp/s13360-022-03209-1.
[35] X. Yang, Y. Xiao, S. Wang, M. Zhao, Electroosmotic flow of fractional Maxwell fluid in a microchannel of isosceles right-triangular cross-section, Mech. Time-Dependent Mater. (2022) 1–20, https://doi.org/10.1007/s11043-022-09576-7.
[36] H. Hanif, I. Khan, S. Shafie, MHD natural convection in cadmium telluride nanofluid over a vertical cone embedded in a porous medium, Phys. Scr. 94 (2019) 125208, https://doi.org/10.1088/1402-4896/ab36e1.
[37] H. Hanif, S. Shafie, R. Roslan, A. Ali, Collision of hybrid nanomaterials in an upper-convected maxwell nanofluid: a theoretical approach, J. King Saud Univ.-Sci. 35 (2023) 102389, https://doi.org/10.1016/j.jksus.2022.102389.